Dual-Mode Free-Jet Combustor

Charles J. Trefny and Vance F. Dippold III
charles.j.trefny@nasa.gov
NASA Glenn Research Center
Cleveland, Ohio
USA

Shaye Yungster
Ohio Aerospace Institute
Cleveland, Ohio
USA

ABSTRACT

The dual-mode free-jet combustor concept is described. It was introduced in 2010 as a wide operating-range propulsion device using a novel supersonic free-jet combustion process. The unique feature of the free-jet combustor is supersonic combustion in an unconfined free-jet that traverses a larger subsonic combustion chamber to a variable throat area nozzle. During this mode of operation, the propulsive stream is not in contact with the combustor walls and equilibrates to the combustion chamber pressure. To a first order, thermodynamic efficiency is similar to that of a traditional scramjet under the assumption of constant-pressure combustion. Qualitatively, a number of possible benefits to this approach are as follows. The need for fuel staging is eliminated since the cross-sectional area distribution required for supersonic combustion is accommodated aerodynamically without regard for wall pressure gradients and boundary-layer separation. The unconstrained nature of the free-jet allows for consideration of a detonative combustion process that is untenable in a walled combustor. Heat loads, especially localized effects of shock wave / boundary-layer interactions, are reduced making possible the use of hydrocarbon fuels to higher flight Mach numbers. The initial motivation for this scheme however, was that the combustion chamber could be used for robust, subsonic combustion at low flight Mach numbers. At the desired flight condition, transition to free-jet mode would be effected by increasing the nozzle throat area and inducing separation at the diffuser inlet.

Preliminary two-dimensional axisymmetric calculations with ethylene fuel and equilibrium chemistry are presented and discussed. They indicate feasibility of the unconfined supersonic combustion process and reveal shock and viscous losses unique to the free-jet concept. It was shown that variation of the nozzle throat area could be used to modify the free-jet shock structure through variation of the pressure in the recirculation zone surrounding the jet. Shocks were also initiated locally within the jet by combustion which began immediately at the inflow plane due to the equilibrium chemistry assumption. Performance and heat load assessments are described.

Follow-on work that refines the initial equilibrium results to include the effects of finite-rate chemistry, and non-uniform fuel-air inflow profiles to more accurately assess ignition characteristics and combustion efficiency is presented. These calculations were carried out at a Mach 8 flight condition with ethylene fuel. V-gutter flameholders were used to initiate combustion at the combustor inflow station. Various fuel-air ratio profiles were imposed a short distance upstream of this plane to simulate upstream fuel injection. The effect of these profiles on thrust, wall heat flux and solution stability are presented. An unexpected result was an unsteady, periodic solution caused by intermittent ignition for some cases with a combustible mixture near the free-jet boundary. These results are included along with the recourse employed to stabilize the flowfield. Results with a smaller combustor diameter, relevant to a Mach 8 point design with reduced heat load and frontal area are presented. Also included are results at Mach 6 and 10 flight conditions for the same geometry. This was done to assess the feasibility of a fixed-geometry flowpath over this Mach number range. Plans for higher fidelity three-dimensional calculations with discrete fuel injection are outlined.

Keywords: Airbreathing Propulsion; Supersonic Combustion Ramjet

NOMENCLATURE

M	Mach number
T	Temperature
A	Cross-sectional area
P	Pressure
R	Radius
V	Velocity
x	Axial distance
$\dot{m}$	Mass rate of flow

Symbols

β	Skewness parameter in formula for Gaussian fuel profile
Φ	Fuel-air equivalence ratio

Subscripts

0	Freestream condition
1	Station 1 (x = 0), inlet throat and free-jet combustor inflow plane
8	Station 8, free-jet combustor nozzle throat
A	Air
EQ	Equilibrium
T	Total (stagnation) condition
max	Maximum

1.0 INTRODUCTION

The potential for high speed and long range has driven aircraft designers to consider airbreathing propulsion since the dawn of high speed flight. The requirement for ever higher flight Mach number spurred development of ramjet propulsion. As the hypersonic flight regime was being explored, issues with the subsonic combustion ramjet cycle and implementation became apparent. These included materials limitations due to the severe stagnation conditions encountered in the combustion chamber, prohibitive momentum losses in the compression process, and impractical variable geometry requirements for the inlet and nozzle. It was recognized by early pioneers in high speed airbreathing propulsion[1,2,3] that these problems could be relieved in a flowpath designed for supersonic combustion. Figure 1 is a diagram from reference 1 that shows the general layout of a supersonic combustion ramjet.

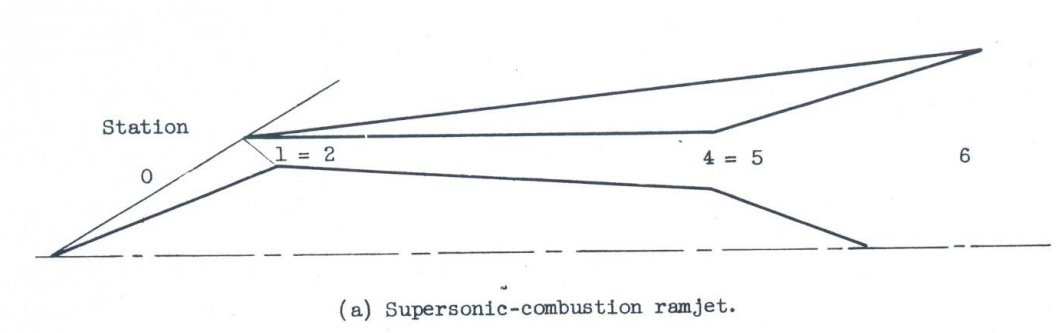

Figure 1. – Diagram of a supersonic combustion ramjet from reference 1.

In general, the cross-sectional area of the supersonic combustor increases in the downstream direction to avoid thermal choking and excessive pressure gradients. Processes that govern performance include inlet momentum losses, Rayleigh losses due to heat addition, heat loss to the combustor walls, skin friction, and chemical non-equilibrium. Other factors that must be considered include separation of boundary-layers due to adverse pressure gradients, intense local heating at re-attachment points and shock impingements, and fuel staging or variable geometry to accommodate the variation of combustion area ratio required with changes in freestream stagnation enthalpy. Airframe integration is also critical, as in using the vehicle forebody for compression and aft-body for expansion of the propulsive stream.

The supersonic combustion ramjet or "scramjet" as it became known, cannot generate thrust at low flight Mach numbers, thus requiring some other means of acceleration to its operating condition. To this end, Curran and Stull[4] introduced the "Dual Mode Supersonic Combustion Ramjet Engine" in a 1972 US Patent that proposed operation in a thermally-choked, subsonic combustion mode at low flight Mach numbers. A diagram from the patent appears in figure 2 where it can be seen that fuel is introduced upstream in supersonic combustion mode at high flight Mach numbers, and downstream in a larger cross-sectional area at low flight Mach number where the heat of combustion is sufficient to form a thermal throat and back-pressure the system.

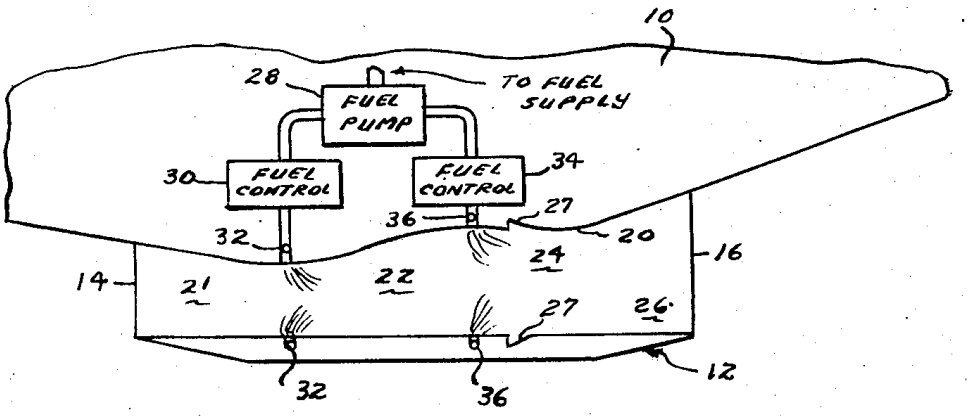

Figure 2. – "Dual Mode Supersonic Combustion Ramjet Engine" from reference 4.

The cross-sectional area at which the thermal throat must form, increases as flight Mach number decreases, unless the fuel-to-air ratio is reduced. For a given duct, this effect determines the minimum flight Mach number for thermally-choked operation. At Mach 3, the required thermal throat area approaches that of the inlet capture area and it could be surmised that combustion extend into the nozzle expansion region. The primary technical challenges in practical application of the dual-mode scramjet scheme are modulation of the thermal throat location, fuel distribution, and ignition and flame-holding in the large cross-section. Any in-stream devices must be retractable or expendable so as not to inhibit supersonic combustion operation.

The free-jet combustor concept was introduced in 2010[5] for application to a wide operating range propulsion system. An alternative to the dual-mode scheme described above, it evolved from a reversal of thinking if you will; a ramjet that operates in a supersonic combustion mode, instead of a scramjet with a thermal throat that forces subsonic combustion. The unique feature of the free-jet combustor pictured in figure 3a, is supersonic combustion in an unconfined free-jet that traverses a larger subsonic combustion chamber to a variable area nozzle throat. During this mode of operation, the propulsive stream is not in contact with the combustor walls, and equilibrates to the surrounding combustion chamber pressure. Qualitatively, a number of possible benefits to this approach are as follows. The combustion process within the jet is augmented by shock waves or potentially oblique detonation waves without regard for the cross-sectional area constraint imposed by walls. Shock wave / boundary-layer interactions, causing localized intense heating and combustor-inlet interaction are eliminated. Inlet flow uniformity requirements are relaxed. Variation in the combustor cross-sectional area distribution, required with flight condition and throttle setting changes, is accommodated aerodynamically by the free-jet without the need for fuel staging. Only the nozzle throat area, through which the jet must issue, is varied. Introduction of a secondary flow to the combustion chamber surrounding the jet may be used to reduce wall temperature and increase the combustion chamber pressure, thereby providing additional aerodynamic contraction. To a first order, thermodynamic efficiency is similar to that of a "traditional" scramjet under the assumption of constant-pressure combustion.

The dual-mode aspect of this device is that the combustion chamber would operate efficiently as a subsonic combustion ramjet to low flight Mach number as pictured in figure 3b. Fuel is injected upstream of the terminal shock, followed by diffusion, subsonic combustion, and a choked nozzle. Ignition and flame-holding would be accomplished with a v-gutter arrangement as shown at the subsonic diffuser exit, with the requirement that this flameholder array must be compatible with operation in the supersonic free-jet mode. A deployable, or even sacrificial flameholder design might be considered. Performance in this mode is that of a subsonic combustion ramjet. At the desired flight condition, transition to free-jet mode is effected by increasing the nozzle throat area to induce separation at the diffuser inlet as the terminal shock system becomes super-critical.

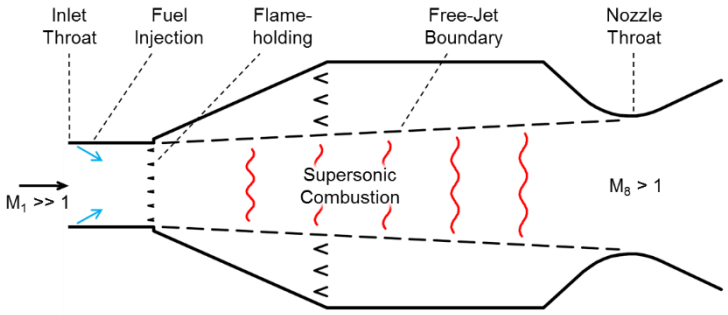

a) Supersonic free-jet combustion mode.

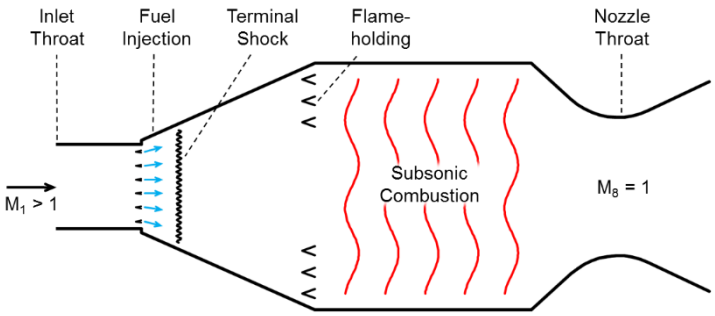

b) Subsonic combustion ramjet mode.

Figure 3. – Free-jet dual-mode combustor.

The initial work, reported in reference 5, included sizing of the combustion chamber and nozzle throat areas for operation over the flight Mach number range of 2.5-12. Computational fluid dynamic (CFD) analysis focused on the free-jet mode of operation, to assess its validity. These calculations were done in two-dimensional, axisymmetric fashion with equilibrium chemistry and ethylene fuel. It was shown that the supersonic free-jet combustion process and fluid mechanics were viable at Mach 5, 8, and 12 flight conditions under the equilibrium chemistry assumption. Varying the nozzle throat area from its design value yielded interesting effects on the free-jet. Encouraged by these results, a second CFD campaign was initiated using a different solver with a finite-rate chemistry model to remove the "mixed-is-burned" assumption tacit in the equilibrium chemistry results. Again, only the free-jet mode of operation was studied using a similar axisymmetric geometry with the fuel and air pre-mixed to varying degrees at the combustor inlet. These results, reported in reference 6, were also encouraging and led to the initiation of a three-dimensional (3D) CFD study to further increase fidelity by modeling the fuel injection and mixing processes of discrete fuel injectors.

The purpose of the present paper is to provide a summary and highlights of the equilibrium and finite rate axisymmetric CFD results, as well as interesting comparisons between the two calculation sets. A description and status of the on-going 3D calculations is also presented.

2.0 CFD ANALYSIS WITH EQUILIBRIUM CHEMISTRY

2.1 Flowpath Sizing and Flight Conditions

Inlet conditions for flight Mach numbers of 5, 8, and 12 were based on a constant 1500psfa dynamic pressure flight trajectory and a nominal inlet performance schedule. These were used in conjunction with the Ramjet Performance Analysis (RJPA)[7] program to determine the appropriate nozzle throat areas based on the constant-pressure combustion of a stoichiometric ethylene-air mixture. The combustor cross-sectional area was sized to accommodate subsonic-combustion ramjet operation at Mach 2.5 and has little to do with the supersonic free-jet mode of operation. Additional details of the design process can be found in reference 5. Table 1 presents the combustor inflow conditions and flowpath area ratios relevant to the present discussion.

Table 1
Freestream and combustor inlet conditions, key area ratios and flow parameters

Flight Mach Number, M_0	Freestream Stagnation Temp, $T_{T,0}$ (R)	Aerodynamic Contraction Ratio, A_0/A_1	Pressure Recovery, $P_{T,1}/P_{T,0}$ (lb/in^2)	Inflow Pressure, P_1 (lb/in^2)	Inflow Temp, T_1 (R)	Inflow Velocity, V_1 (ft/sec)	Inflow Mach Number, M_1 (ref)	Nozzle Area Ratio, A_8/A_1	Air Flow Rate, $\dot{m}_a$ (lb/sec)	Ethylene-Air Equilibrium Temperature $T_{T,EQ}$ (R)
5	2,225	9.9	0.605	27.26	1321	3509	2.00	3.743	97.4	5,074
6	2,982	*14.0	0.493	*30.65	*1594	*4428	*2.30	*2.709	95.4	5,428
8	4,833	16.0	0.288	21.77	1966	6531	3.08	2.709	81.1	6,360
10	7,163	*17.8	0.139	*19.98	*2609	*8379	*3.45	*2.709	71.9	7,717
12	10,085	23.2	0.060	25.29	3714	10055	3.51	1.833	63.2	9,682

* Based on Mach 8 geometry

Ethylene fuel was injected axially at the x=0 inflow station through three annular, sonic slots, except for the Mach 5 case where two slots were used due to choking in the cylindrical inlet section. These slots were of equal width and were placed at the center of equal-width annuli to give the same fuel-air ratio in each region. Figure 4 depicts the geometry used for the equilibrium calculations at the Mach 8 flight condition. Variation in inlet and nozzle throat area required for the Mach 5 and 12 flight conditions is accomplished only schematically for the axisymmetric geometry assumed herein. The nozzle expansion section downstream of the throat (station 60.575) is there only to facilitate application of a downstream boundary condition. Net thrust is calculated using RJPA based on ideal expansion to freestream pressure of the mass-averaged flow state at the throat.

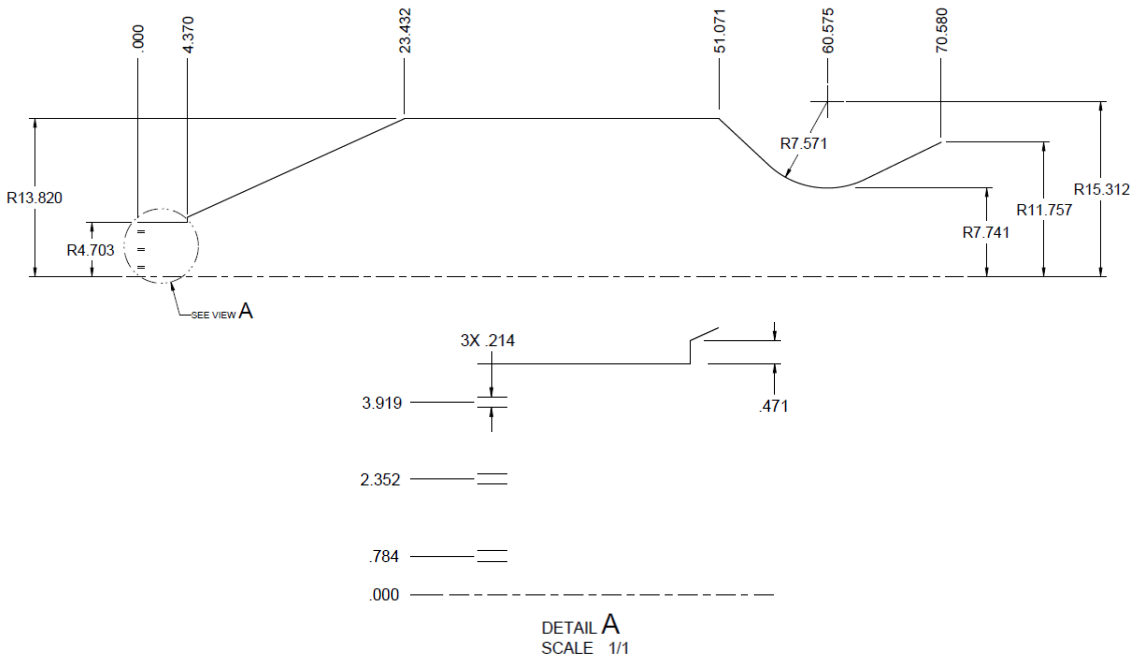

Figure 4. – Geometry and fuel injection slot detail used for simulation with equilibrium chemistry. Mach 8 flight condition shown (dimensions in inches).

2.2 CFD Method

The GASP[8] CFD code was used for these simulations. The Reynolds-Averaged Navier-Stokes equations were converged using the 3rd-order, upwind-biased Roe scheme. Fully turbulent flow was assumed using the Menter Shear Stress Transport (SST) turbulence model with compressibility correction. The eight-species, three-reaction Baurle ethylene-air chemistry model was used in equilibrium chemistry mode where infinite reaction rates are assumed. Walls were treated as adiabatic except for a number of runs made with constant wall temperature to evaluate heat load. The grid consisted of 414,000 grid points. More details of the grid and analysis assumptions are available in reference 5.

2.3 Results at Mach 5, 8, and 12 Flight Conditions

The initial objective of these calculations was to assess the feasibility of combustion in a supersonic free-jet, and the jet's ability to reattach to a flow surface at the nozzle throat. Thrust performance, in light of the surrounding recirculation zone, and the heat load of the relatively large diameter combustion chamber were also of primary interest. Calculations at the Mach 5, 8, and 12 flight conditions converged to steady-state and revealed interesting features of the supersonic free-jet combustion process.

Figure 5 shows that mixing and heat release begin at the x=0 inflow plane with depletion of the fuel and an immediate increase in mass-averaged pressure. The fuel was completely mixed and burned in the distance between the inlet and nozzle throat stations. The Mach 5 case used two injection slots to reduce the rate of heat release in the axial direction and this is evident in figure 5a. Temperature contours in figure 6 show the effect of ethylene combustion in the jet, and also that the recirculation zone equilibrates to roughly 90% of the ethylene-air equilibrium temperature for the Mach 8 and 12 cases. The recirculation zone in the Mach 5 case was significantly cooler. This was attributed to less fuel being entrained into the shear layer with the two-injector arrangement. This was a significant finding and informed the fuel-injection schemes that were investigated in subsequent studies.

Given the relatively smooth, mixing-limited character of the ethylene fuel depletion and heat release, pressure traces in figure 5b and contours in figure 6 retain the periodic signature of an off-design supersonic jet. As expected, the wavelength of the pressure signatures lengthen as the flight and corresponding inlet Mach numbers increase. The pressure ratio, P/P_1, in the recirculation zone surrounding the jet, indicated numerically in the pressure field, equilibrated to a value greater than one in all cases. Recall that the nozzle throat area was sized for constant-pressure combustion at the inflow pressure (P_1) and is now off-design due to pressure rise in the inlet section. In all cases, the free-jet re-joins the nozzle throat contour near the 60-in. station. The periodic nature of the jet now makes significant the axial location of the nozzle throat. An interaction of varying intensity occurs, depending on whether or not the shock structure and streamlines are in phase with the geometry. In the Mach 8 case, the streamlines appear to be unaffected as the jet smoothly re-joins the nozzle contour, however in the Mach 12 case, the streamlines are deflected towards the axis and a strong shock appears.

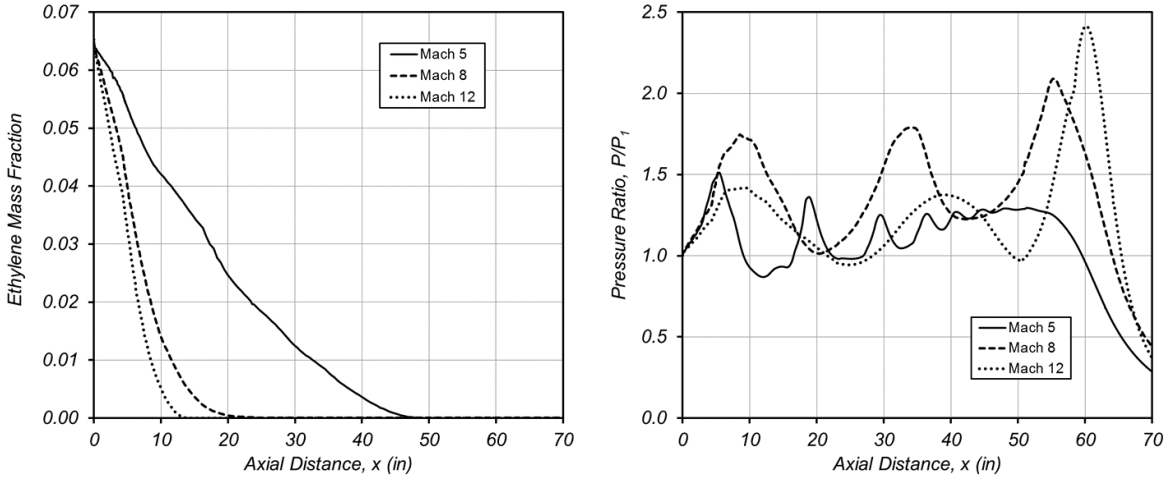

a) Ethylene mass fraction distributions

b) Pressure distributions

Figure 5. – Mass-averaged quantities as a function of axial distance for Mach 5, 8, and 12 flight conditions; GASP equilibrium chemistry.

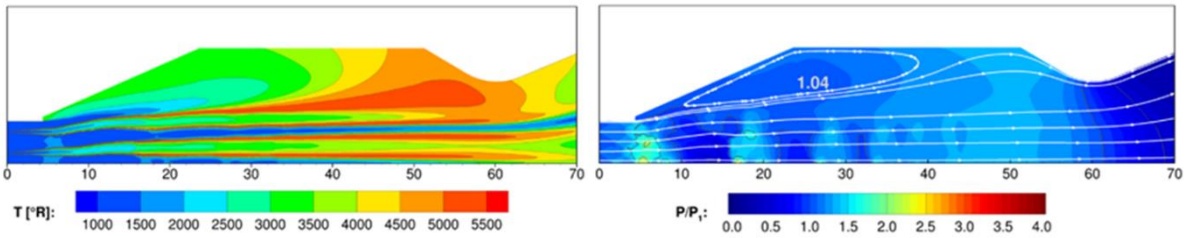

a) Mach 5 flight condition (2 injectors)

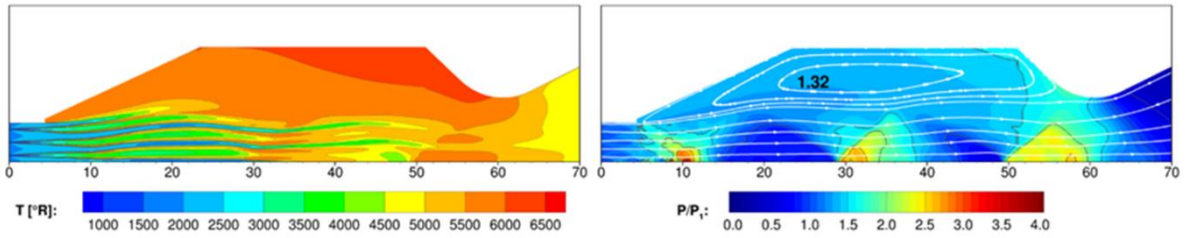

b) Mach 8 flight condition (3 injectors)

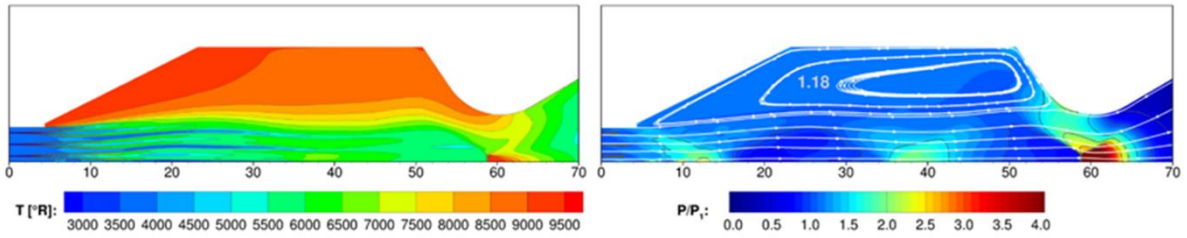

c) Mach 12 flight condition (3 injectors)

Figure 6. – Contours of temperature and pressure for Mach 5, 8, and 12 flight conditions. Pressure ratio P/P_1 in the recirculation zone is indicated numerically in the pressure field; GASP equilibrium chemistry.

2.4 Effect of Nozzle Throat Area on Results at the Mach 8 Flight Condition

Given the significant wave structure in the jet and with the realization that the design nozzle throat areas may not be optimum, additional calculations were done with 80, 90, and 110% of the design throat area for the Mach 8 flight condition.

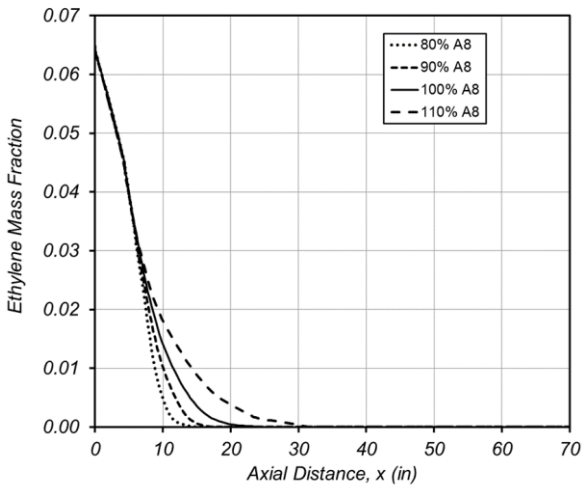

a) Ethylene mass fraction distributions.

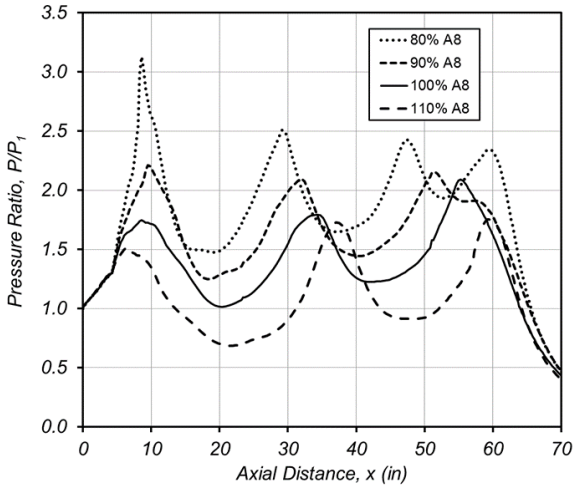

b) Pressure distributions.

Figure 7. – Mass-averaged quantities as a function of axial distance for various nozzle throat area ratios. Mach 8 flight condition; GASP equilibrium chemistry.

The effects of reducing the nozzle throat area are to increase the overall pressure level in the combustion chamber and to modify the wave structure in the jet. Figure 7a shows the relative insensitivity of nozzle throat area to mixing and combustion of the ethylene fuel. The expected trend of more vigorous mixing as pressure increases is evident. Figure 7b shows the overall increase in mass-averaged pressure as the nozzle throat area is reduced. The more interesting effect however, is the reduction in wavelength of the shock structure that begs a comparison between it and the fixed nozzle throat location. The 100% throat area trace is in phase with the nozzle throat location, and this is corroborated by the pressure contours in figure 8c, where the streamlines smoothly join the throat contour. The 80% case is clearly not in phase, as the final peak is forced upstream by the nozzle contraction resulting in the strong shock on the axis in figure 8a. The nozzle contraction also causes an inflection in the 90% pressure trace, causing the relatively mild interaction seen in figure 8b. The 110% case is almost in phase, but close examination of figure 7b reveals a discontinuity in pressure at the 57-inch station, consistent with the strong shock on the axis in figure 8d.

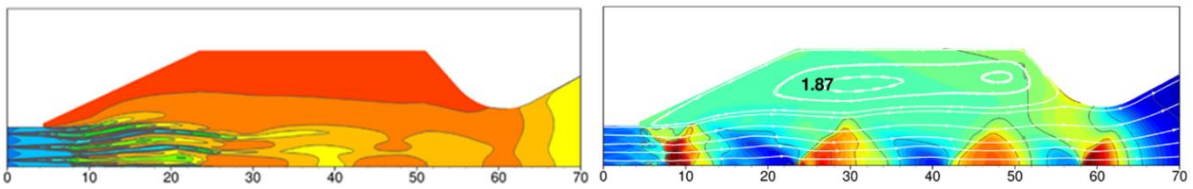

a) Nozzle throat area, A_8 = 80% of design value.

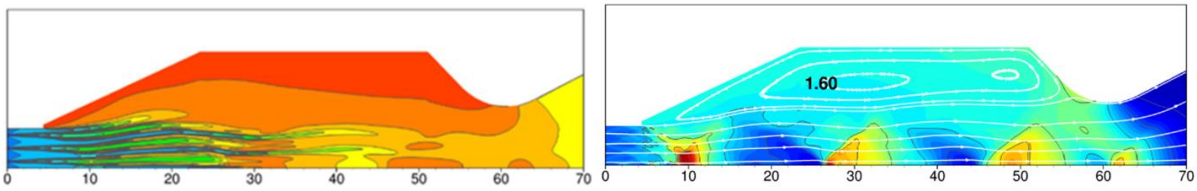

b) Nozzle throat area, A_8 = 90% of design value.

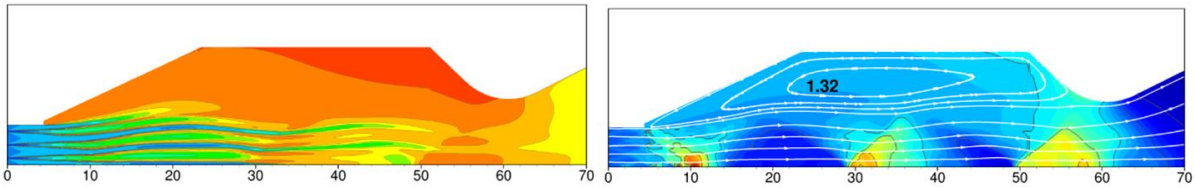

c) Nozzle throat area, A_8 = 100% of design value.

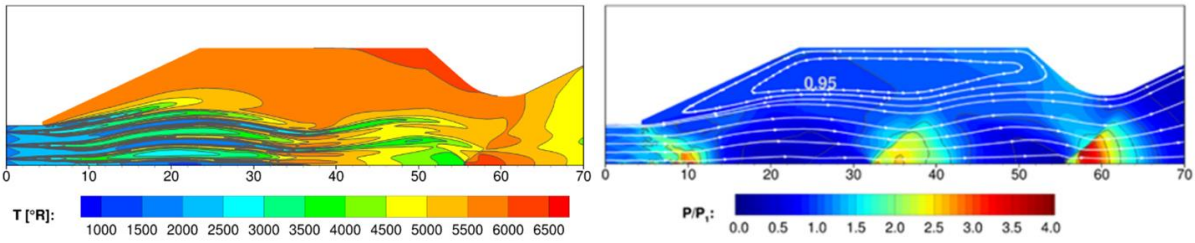

d) Nozzle throat area, A_8 = 110% of design value.

Figure 8. – Contours of pressure and temperature for various nozzle throat area ratios for the Mach 8 flight condition; GASP equilibrium chemistry.

Figure 7b also shows that the increasing combustion chamber pressure does not feed forward of the 4.37-in. station. Temperature contours appearing on the left-hand side of figure 8 show a measurable increase in combustion chamber wall temperature as the nozzle throat area is reduced. These results are significant in that the free-jet combustor operability is relatively insensitive to the throat area, and therefore may be operable over a significant range of flight Mach numbers with fixed geometry.

2.5 Net Thrust and Heat Load Based on GASP Results

To assess performance of the free-jet combustor, and facilitate comparison to an ideal scramjet, the potential net thrust was calculated by assuming an ideal, equilibrium expansion of the mass-averaged properties at the throat to freestream pressure using RJPA. For comparison, a series of companion calculations were done where the

combustor inflow conditions used for the CFD cases were processed through an ideal supersonic combustion process at the same pressure ratios as the CFD results using RJPA, then expanded to freestream pressure under the same assumptions. This reveals the loss in net thrust due to flow features unique to the free-jet combustor. These results appear in figure 9 and show net thrust per unit airflow 12% and 29% below the ideal at Mach 8 and 12 respectively. The variable nozzle throat area cases at Mach 8 appear in the figure simply to show the relative insensitivity of net thrust to nozzle throat area. Worth noting is that the 80% throat area case had the highest net thrust, improving from 70.5 to 73.3 as the positive effect of increasing combustion pressure ratio overcame the more severe shock losses. It is also important to point out that the ideal cases used here for comparison in no way represent the performance achievable with a conventional scramjet combustor as it too would have friction and shock losses, along with the thermal and operability issues related to shock wave / boundary-layer interactions discussed above.

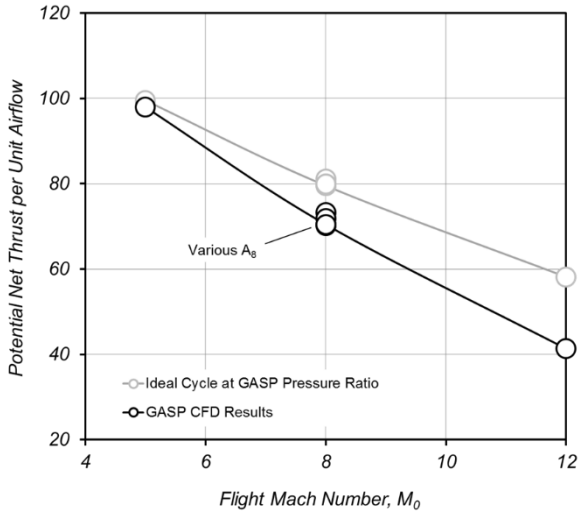

Figure 9. – Net thrust for flight Mach numbers of 5, 8, and 12 based on GASP equilibrium chemistry results.

GASP calculations at the Mach 5, 8, and 12 flight conditions were repeated with a constant-temperature wall boundary condition to assess heat load. Wall temperatures of 2000, 3000, and 4000R were evaluated. Heat load in terms of BTU's per pound of fuel ranged from 2800-3500 at Mach 12, 1000-1500 at Mach 8, and 0-500 at Mach 5. In the interest of brevity, the reader is directed to reference 5 for more detail on the method and results of these calculations. Heat loads were also evaluated during the second CFD campaign where steps were taken to reduce them to values manageable with hydrocarbon fuels. These will be presented in a subsequent section.

3.0 CFD ANALYSIS WITH FINITE-RATE CHEMISTRY

The GASP equilibrium calculations proved the viability of supersonic free-jet combustion, and its application to airbreathing propulsion. They also revealed interesting interactions between the free-jet, its surrounding recirculation zone, and the nozzle throat geometry. However, some lingering doubt remained due to the simplifying assumptions used in these calculations. The objectives of the next CFD campaign were to determine the effects of finite-rate chemistry, and explore means to reduce the combustion chamber heat load. Calculations were focused on the Mach 8 flight condition, but were also done to explore the feasibility of a fixed geometry system over the flight Mach number range of 6 to 10. Use of a smaller diameter combustion chamber, relevant to a Mach 8 point design, was also studied. These results were reported in reference 6 and will be summarized here along with work completed subsequently. Inlet conditions and other relevant parameters for flight Mach numbers of 6, 8, and 10 were based on the same flight trajectory as the GASP calculations, and appear in table 1.

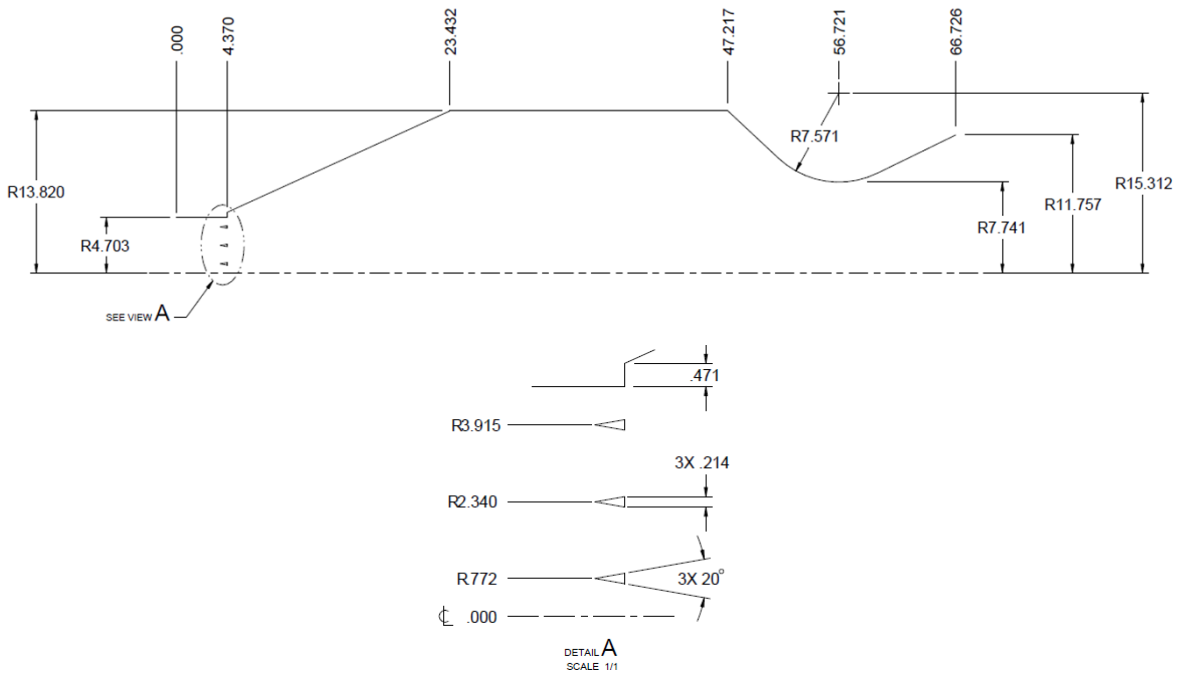

Figure 10. – Geometry and flameholder detail used for simulation with finite-rate chemistry. Mach 8 flight condition shown (dimensions in inches).

A diagram of the flowpath appears in figure 10. It was similar to that used for the GASP calculations with the following exceptions. The fuel injectors used in the GASP simulation were eliminated in favor of a pre-mixed stream of fuel and air. Uniform and non-uniform fuel profiles, all of overall stoichiometric proportion were imposed at the inflow station at x=0. A skewed Gaussian function was used to generate the non-uniform profiles shown in figure 11 where the parameter β determines the degree of non-uniformity. These profiles were intended to give a fuel lean condition in the free-jet shear layer to reduce heat load. The pre-mixed approach was also intended to mimic the result of upstream fuel injection that was not modeled in this analysis. Note that varying degrees of mixing are required for complete combustion with the non-uniform cases. These profiles will be referred to subsequently by their maximum equivalence ratio (Φ_{max} = 1.5, 2.5, or 3.5). V-gutter flameholder rings were added at the end of the cylindrical inflow section at station 4.37-in. The total base area of the three flameholders was 9.45 in^2 and represents a blockage of 13.6% of the inflow area. Finally, the cylindrical combustion chamber was made somewhat shorter to further reduce heat load.

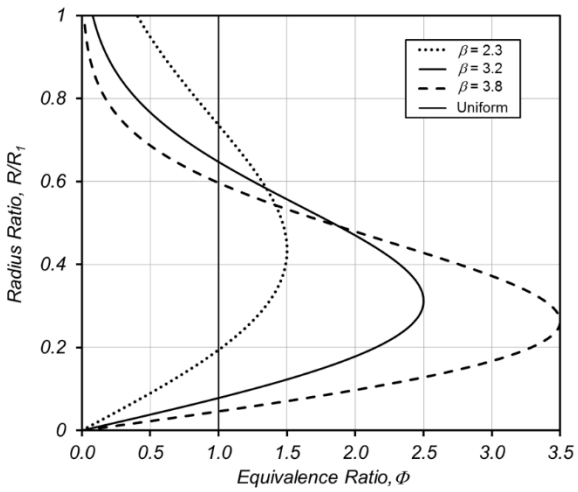

Figure 11. – Fuel-air ratio profiles imposed at the inflow plane (x = 0).

3.1 CFD Method

Calculations were carried out using a time-accurate, fully-implicit (TAFI) code developed in-house. The reader is referred to references 9 and 10 for details of the numerical methods used. The axisymmetric, unsteady, Reynolds-Averaged Navier-Stokes equations were solved for a multi-species, thermally-perfect, chemically-reacting gas. The Spalart-Allmaras one-equation turbulence model was used with a constant value of 0.9 for the turbulent Prandtl and Schmidt numbers. Adiabatic and constant temperature wall boundary conditions were considered. A reduced ethylene-air combustion mechanism, developed by Singh and Jachimowski[11] was used, consisting of 10 elementary reactions among 9 reacting species.

The grid consisted of 24 blocks with a total of approximately 136,840 grid points. The minimum wall distance for adiabatic wall calculations was set to 2.0×10^{-3} inches resulting in y+ values of order one. For constant wall temperature calculations, a reduction in wall spacing to 2.0×10^{-4} inches was required for the computed heat flux coefficients to be within 10% of the asymptotic value. More details of the grid and analysis assumptions are available in reference 6.

3.2 Effect of Inflow Equivalence Ratio Profile on Results for the Mach 8 Flight Condition

The initial calculation was done with a uniform fuel inflow profile. This solution, and a second using the $1.5\Phi_{max}$ profile converged to a periodic state. This is attributed to high sensitivity of ignition delay to temperature at the local conditions near the flameholders, and coupling of the free-jet shock structure to the combustion chamber pressure. This is discussed further in reference 6 where contour plots for both the maximum and minimum pressure conditions are presented. Time histories of pressure at a point in the combustion chamber recirculation zone for these two cases appear in figure 12, where it is evident that the $1.5\Phi_{max}$ fuel profile reduced the amplitude of the pressure signal by approximately 60%, while slightly increasing the wavelength.

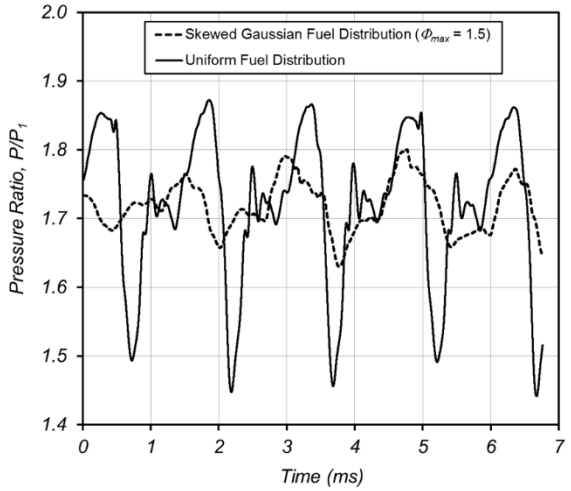

Figure 12. – Time histories of recirculation zone pressure, Mach 8 flight condition with uniform and low Φ_{max} inflow fuel profiles; TAFI finite-rate chemistry.

Subsequent runs with 2.5 and 3.5 Φ_{max} profiles yielded steady solutions due to the wider range of local Φ in the ignition zones that require mixing for combustion, and lessen the sensitivity of the combustion process to ignition delay. The mixing effect is evident in the ethylene mass fraction contours of figure 13 as the downstream persistence of ethylene increases with Φ_{max}. Combustion efficiency approaches 100% for all cases except at the highest Φ_{max} where roughly 5% of the fuel remains unburned at the nozzle throat. In reference 6, it is shown that reducing the nozzle throat area to 80% of its baseline value also stabilized the uniform inflow solution by increasing the local temperature at the flameholders, which also reduces the sensitivity to ignition delay time.

The temperature contours of figure 13 show the desired reduction in recirculation zone temperature with increasing Φ_{max} as the fuel-air ratio in the shear layer is reduced. This is a key result, and as will be shown in a subsequent section, results in a significant reduction in heat load.

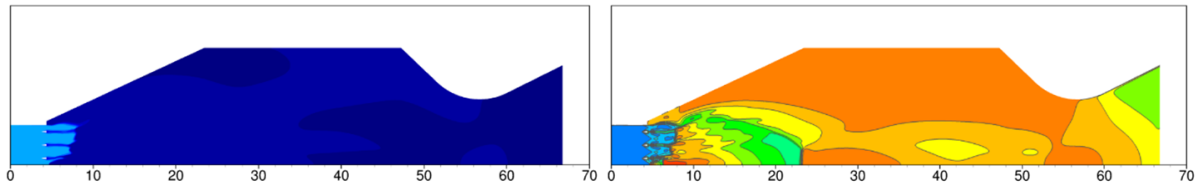

a) Uniform inflow (periodic, near high pressure peak).

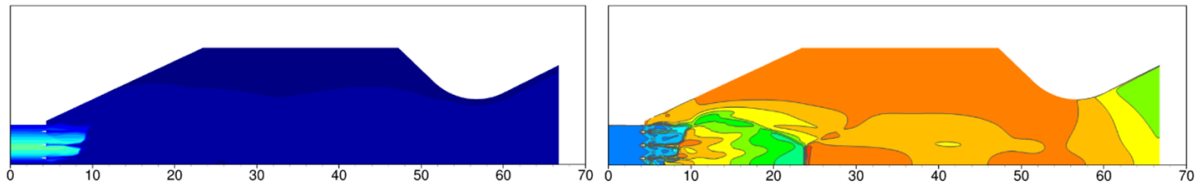

b) Φ_{max} = 1.5 (periodic, near high pressure peak).

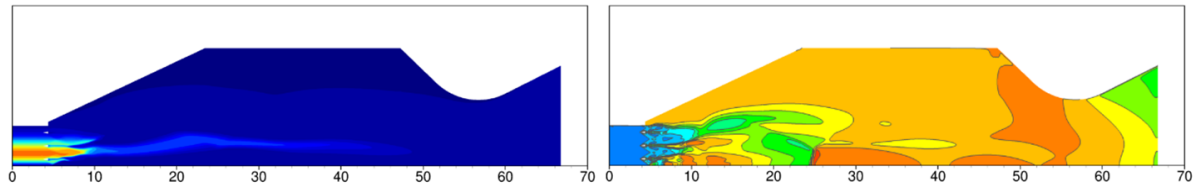

c) Φ_{max} = 2.5 (steady)

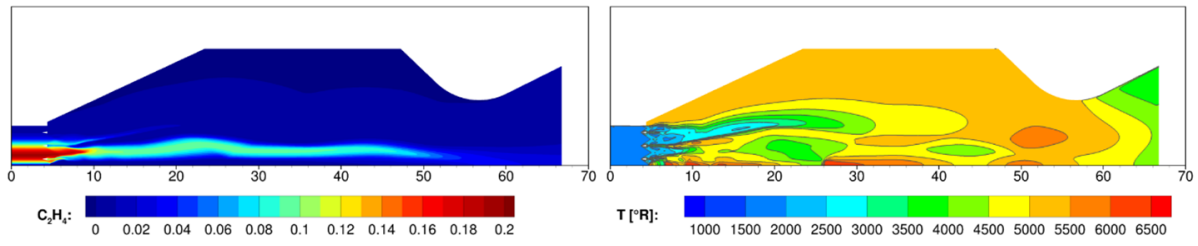

d) Φ_{max} = 3.5 (steady)

Figure 13. – Results with various inflow Φ profiles, Mach 8 flight condition; TAFI finite-rate chemistry.

3.3 Effect of Inflow Equivalence Ratio Profile on Results for Mach 8 Flight Conditions

Figure 14 presents solutions at 80, 100, and 120% of the design nozzle throat area with the 2.5 Φ_{max} inflow profile. The effects of varying the nozzle throat area are similar to those of the GASP simulations. Reducing the nozzle throat area increases the combustion chamber pressure and temperature, and wavelength of the shock structure in the free-jet. However combustion chamber pressures equilibrated to significantly higher values than those of the GASP equilibrium chemistry calculations in figure 8. This is indicative of greater momentum losses in the jet that cause the nozzle throat area to be even further off-design. It is important to note however, that the strong network of shock waves induces ignition and combustion in a short distance, and that this would be highly impractical in a traditional "walled" combustor. A significant difference between the TAFI and GASP calculations is apparent by comparing the mass-averaged ethylene distributions of figures 15a and 7a. Ethylene depletion in the finite rate case has the step-wise signature of a shock-induced process, as opposed to the more gradual mixing characteristic seen in the equilibrium chemistry simulations. Roughly 85% of the fuel is consumed at the first shock in the 80 and 100% A_8 cases with the balance requiring mixing downstream. The 120% A_8 case has a second shock-induced feature from 25 to 30-inches.

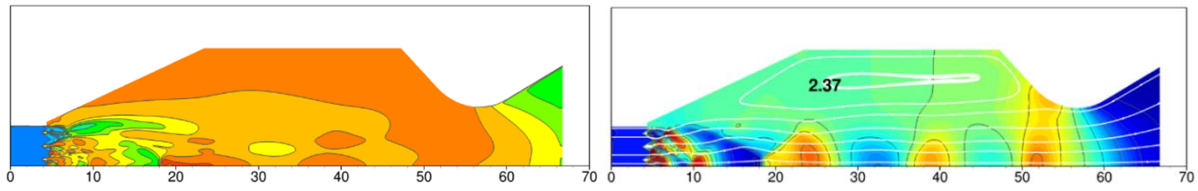

a) Nozzle throat area, A_8 = 80% of design value.

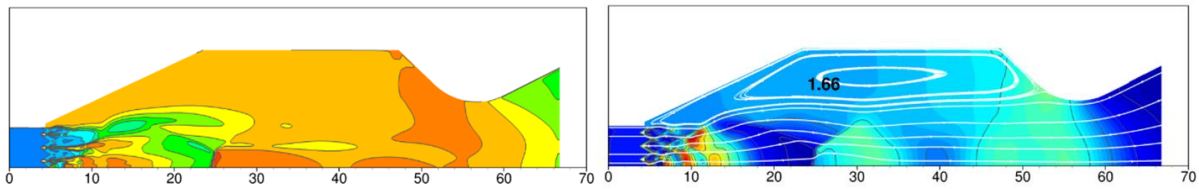

b) Nozzle throat area, A_8 = 100% of design value.

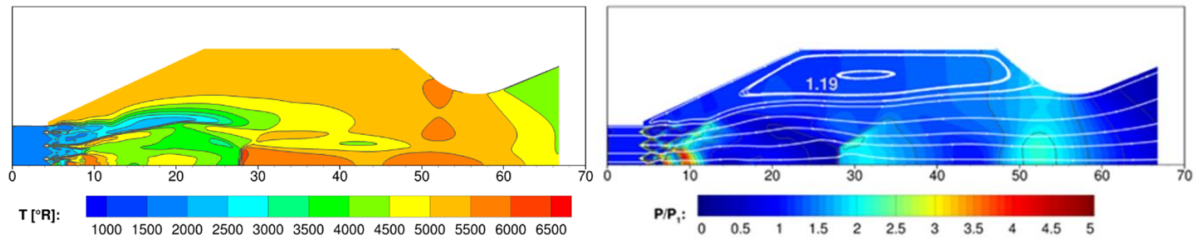

c) Nozzle throat area, A_8 = 120% of design value.

Figure 14. – Effect of nozzle throat area on temperature and pressure fields, Mach 8 flight condition, 2.5 Φ_{max} inflow profile; TAFI finite-rate chemistry.

Mass-averaged pressure distributions in figure 15b clearly show the strong shocks just downstream of the flameholder array in the 80 and 100% A_8 cases, with less intense features at 120%. The non-linear nature of the heat release also results in a less regular periodicity in the pressure traces than seen for the equilibrium calculations in figure 7.

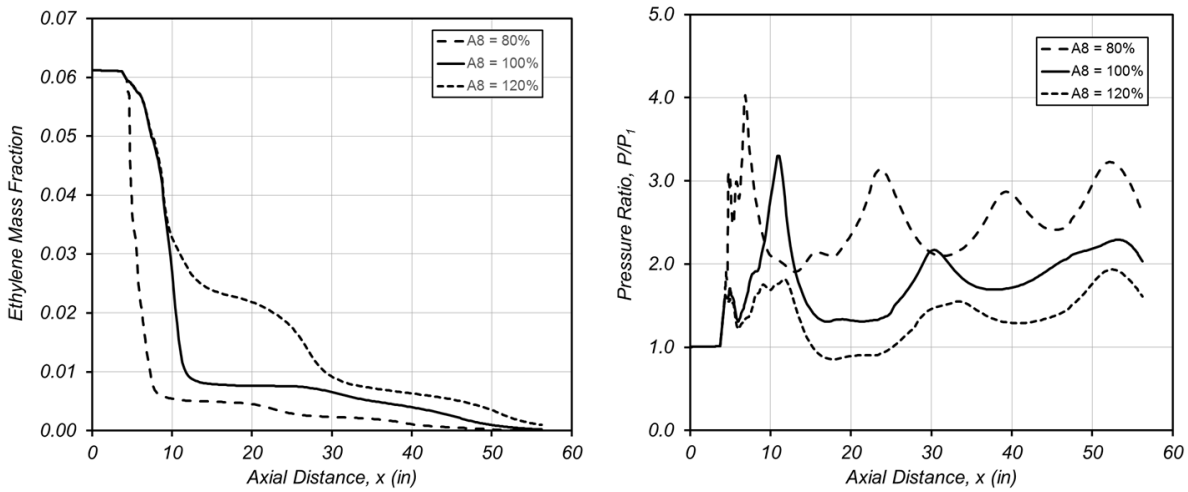

a) Ethylene mass fraction distributions.

b) Pressure distributions.

Figure 15. – Mass-averaged quantities as a function of axial distance for various nozzle throat area ratios. Mach 8 flight condition; TAFI finite-rate chemistry.

3.4 Results with Single Flameholder

Given that shock waves in the off-design free-jet had significant influence on the ignition and combustion processes, a configuration with a single flameholder was considered, again with a 2.5 Φ_{max} fuel inflow profile at the Mach 8 flight condition. Figure 16 compares these results to those with three flameholders. Differences in ethylene mass fraction are almost imperceptible, reinforcing the conclusion that shock-induced combustion is the dominant mechanism. There is more significant difference in the pressure field, where a weaker shock network is evident near the flameholders in the single flameholder case. Also of note is that a lower momentum deficit in the single flameholder case reduces the pressure ratio in the combustion chamber from 1.66 to 1.55. Recall that this pressure ratio was 1.32 for the comparable GASP simulation in figure 8c. Temperature contours show little difference between the one and three flameholder cases.

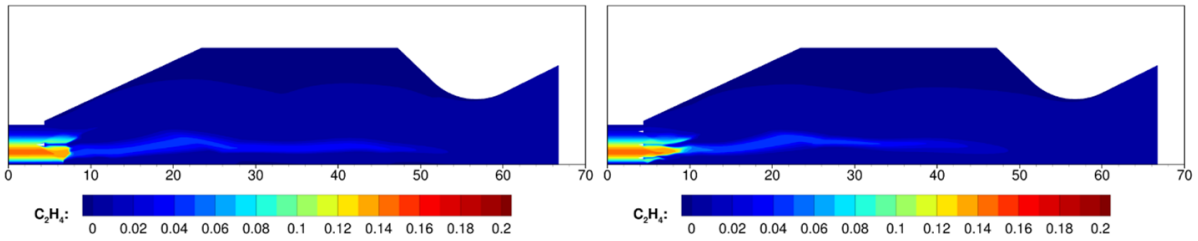

a) Ethylene mass fraction (three-flameholder case on the right).

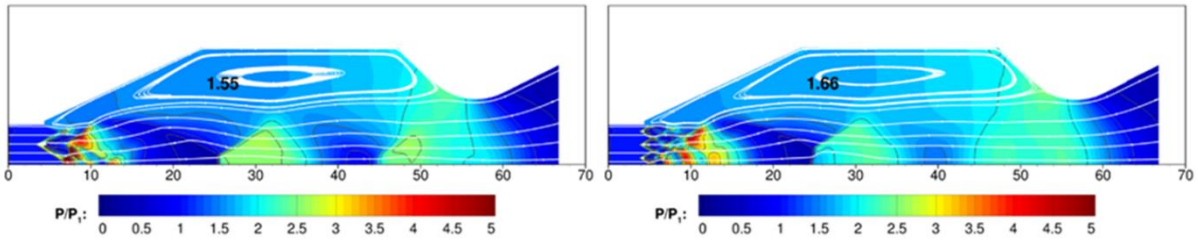

b) Pressure and streamlines (three-flameholder case on the right).

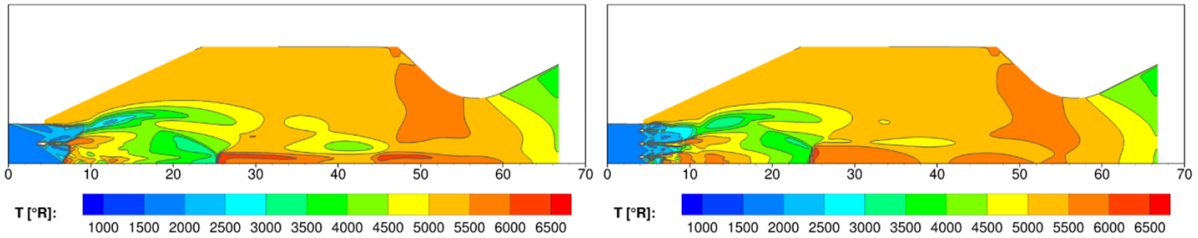

c) Temperature (three-flameholder case on the right).

Figure 16. – Results with a single flameholder compared to the three-flameholder case; TAFI finite-rate chemistry.

3.5 Mach 8 Point Design

With confidence that the supersonic free-jet combustion process was viable, and conceivably more robust than other supersonic-combustion schemes, it was proposed that a Mach 8 point-design would be of interest. Recall that the combustion chamber was sized to accommodate subsonic combustion ramjet operation at Mach 2.5. If other means of acceleration to Mach 8 were available, the combustion chamber diameter could be reduced, with concomitant reductions in frontal area, weight, volume and heat load. A calculation was carried out with a combustion chamber cross-sectional area equal to 60% of the original value (77% diameter). Three flameholders and a 2.5 Φ_{max} inflow profile were used. Results of this calculation are compared to those of the 100% combustion chamber diameter case in figure 17. The most significant differences appear in the pressure field, where the recirculation zone is substantially thinner with greater pressure gradient fore-to-aft. Recirculation zone temperature is slightly higher in the point-design case, and ethylene depletion is almost identical. As will be shown in the next section, reduction of the combustion chamber diameter has negligible effect on thrust, and results in a significant reduction in heat load.

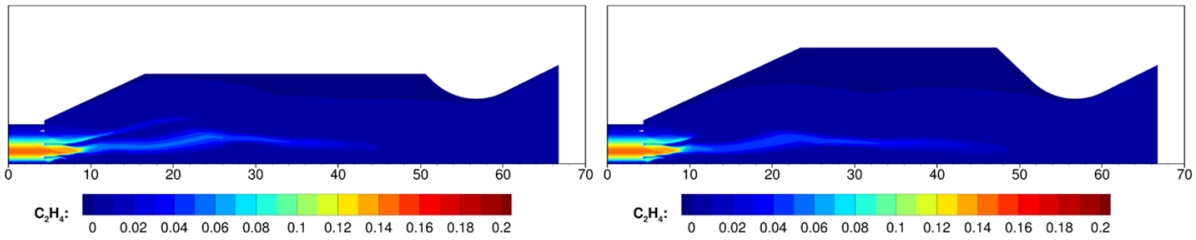

a) Ethylene mass fraction (baseline case on the right).

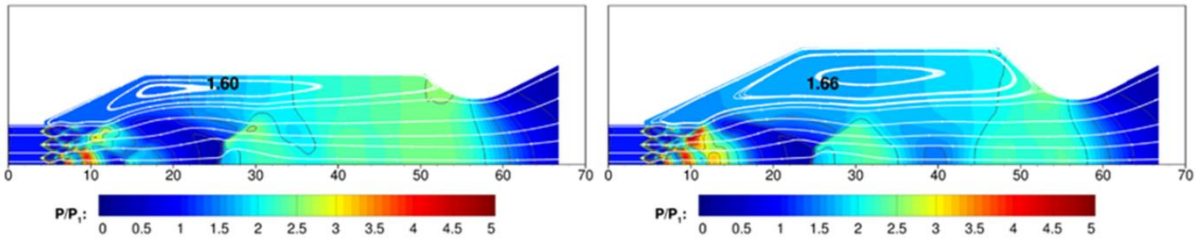

b) Pressure and streamlines (baseline case on the right).

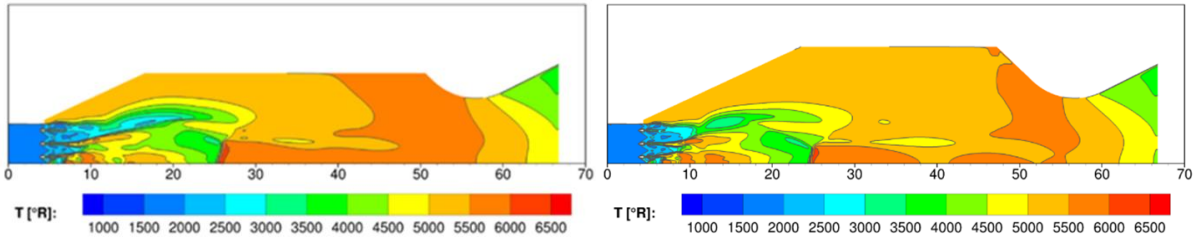

c) Temperature (baseline case on the right).

Figure 17. – Results with 60% combustion chamber cross-sectional area compared to baseline case; TAFI finite-rate chemistry.

3.6 Net Thrust and Heat Load Based on TAFI CFD Results

Figure 18 presents the potential net thrust per unit airflow as a function of combustion pressure ratio based on the TAFI CFD results for the Mach 8 flight condition. Similar to the GASP results discussed earlier, net thrust for the TAFI results was calculated by expanding the mass-averaged properties at the nozzle throat to freestream pressure using RJPA, assuming equilibrium chemistry and no momentum loss. Any ethylene left unreacted at the nozzle throat station was treated as inert in the expansion process. The envelope overlaid in figure 18 shows the performance limits given the inflow state corresponding to the Mach 8 flight condition. At a given pressure ratio, the upper bound is an ideal combustion process wherein the only momentum loss is that due to combustion, and the lower bound represents sufficient momentum loss by shocks and friction to drive the free-jet to a sonic condition at the nozzle throat. Lines of constant area ratio show that net thrust is maximum for a constant area combustion process. The free-jet combustor design point which assumes constant-pressure combustion with a nominal momentum loss appears at a pressure ratio of one. In order to make a comparison between the equilibrium and finite-rate results, the GASP results were corrected to account for the higher fuel inflow momentum of the TAFI calculations. Note that the GASP results do not fall on the expected overlaid area ratios. This is an artifact of mass-averaging the highly distorted supersonic nozzle throat properties. In fact, both the GASP and TAFI results fall on their effective, not geometric, nozzle throat areas calculated by dividing the mass flow rate by the product of mass-averaged density and velocity. Net thrust for the GASP cases is 9-12% below the ideal limit due to shock losses in the free-jet and friction losses associated with the recirculation zone. They do not follow the expected trend of lower pressure ratio with increasing nozzle throat area because of the strong shock that developed at the throat in the 110% A_8 case, increasing the mass-averaged pressure to a value greater than that of the 100% A_8 case. TAFI cases fall 17-23% below ideal, at or near the sonic limit due to increased momentum losses associated with the shock-induced combustion process. Performance of the single-flameholder case indicates that flameholder drag is not a significant contributor to the overall momentum loss. In general, the effect of reducing the nozzle throat area is to raise the pressure level, thereby increasing performance.

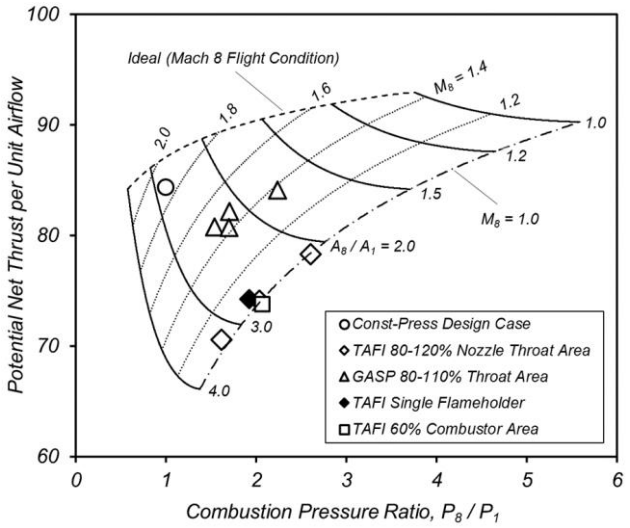

Figure 18. – Comparison of net thrust performance between TAFI and GASP results. Mach 8 flight condition.

TAFI calculations were repeated for selected cases with a finer grid and constant wall temperature to determine the fuel heat load. Refer to reference 6 for details of this procedure. The constant wall temperature boundary condition had negligible effect on the flowfield or performance. Figure 19 presents the fuel heat load as a function of wall temperature for all of the 100% nozzle throat area cases discussed above. Note the significant reduction in heat load with increasing Φ_{max}, as the fuel-air ratio in the free-jet shear layer is reduced. Heat load for the 3.5 Φ_{max} case is 24-39% below that of the 1.5 Φ_{max} case depending on wall temperature. As expected, heat load for the 60% combustor area case scales closely with surface area, and is significantly lower than the corresponding 2.5 Φ_{max} case at 100%. The maximum change in sensible enthalpy for most hydrocarbon fuels heated from room temperature to 1000^0F is 700-800 BTU/lbm.[12] The energy absorbed can be increased substantially by endothermic reaction. For example, the cooling capacity of "cracked" JP-7 increases to 1170 BTU/lbm.[12] Based on these levels, and a Φ_{max} of 2.5, combustor walls can be cooled to 3000^0R with hydrocarbon fuel, and 2000^0R assuming endothermic JP-7.

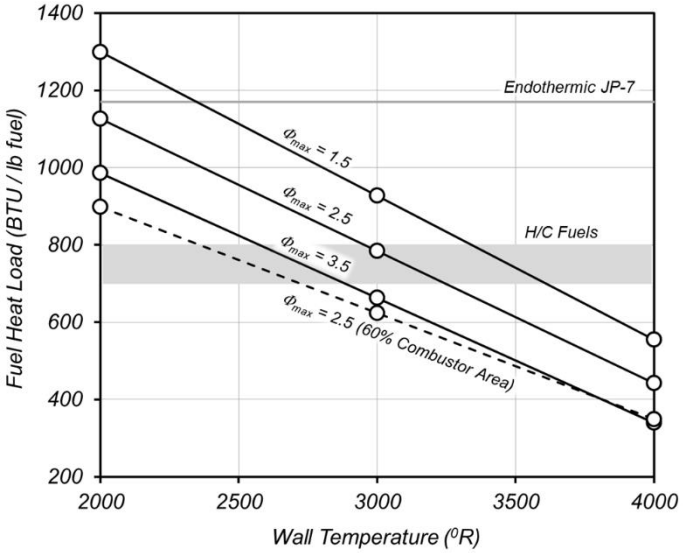

Figure 19. – Effect of inflow fuel-air ratio non-uniformity on fuel heat load for a stoichiometric mixture based on TAFI finite-rate chemistry simulations at the Mach 8 flight condition.

3.7 Results for Baseline Geometry at Mach 6 and 10 Flight Conditions

With the understanding that performance and operability is relatively insensitive to nozzle throat area, it was of interest to run a fixed-geometry system over a substantial flight Mach number range. To this end, calculations at

Mach 6 and 10 flight conditions were carried out using the Mach 8 geometry. With respect to design values, this causes both the inlet and nozzle throats to be over-contracted for the Mach 6 case, and under-contracted for Mach 10. Relevant boundary conditions and geometric parameters for these calculations appear in table 1. In the Mach 6 calculation, a detonation wave formed just downstream of the flameholders and propagated upstream to the inflow boundary. A reduction in equivalence ratio to 0.6 resulted in a stable periodic solution. Although not pursued at the time, reducing the number of flameholders, or increasing the non-uniformity of the fuel inflow profile, might have yielded a stable result at the Mach 6 flight condition. Results of the Mach 10 calculation appear in figure 20 where it is apparent that the ethylene fuel was consumed well upstream of the nozzle throat. Pressure contours and streamlines show the wave structure and lower combustion chamber pressure ratio indicative of the oversized nozzle throat. The ideal net thrust per unit airflow for this case is 50.2. Similar to the results of figure 18, a comparison was made to an ideal calculation at the same combustion pressure ratio and this value is 80.3.

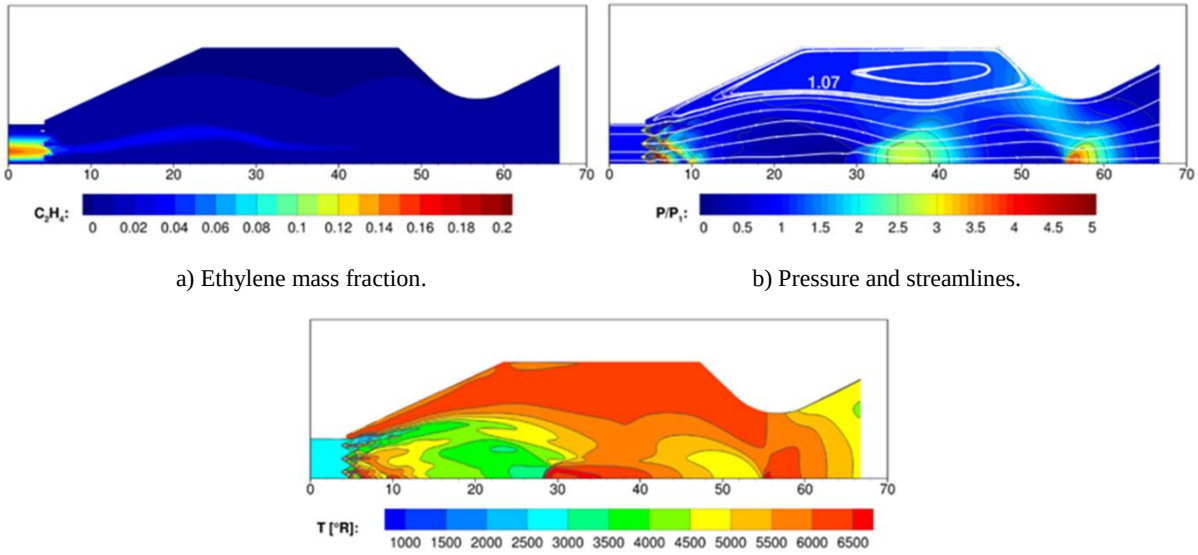

a) Ethylene mass fraction.

b) Pressure and streamlines.

c) Temperature.

Figure 20. – Results for Mach 8 geometry at Mach 10 flight condition. Φ_{max} = 2.5; TAFI finite-rate chemistry.

Results of both the TAFI and GASP calculations provide confidence that neither finite-rate chemistry nor mixing would limit the viability of the supersonic free-jet combustor. In fact, the shock-induced combustion process seen in the TAFI calculations may ultimately make the free-jet scheme a more practical means of supersonic combustion for high flight Mach number applications.

4.0 STATUS OF THREE-DIMENSIONAL CALCULATIONS

An effort is currently underway to extend the analysis to three-dimensions including fuel injection upstream of station 1 using the National Combustion Code (NCC).[13,14] The 3D geometry, shown in figure 21, is similar to the axisymmetric geometry used for the TAFI calculations, except for an extended inlet section with four discrete fuel injectors. The injectors were sized to provide a stoichiometric fuel-air ratio with adequate penetration using the correlation described in reference 15. To date, only the cylindrical inlet section has been gridded, and a non-reacting solution obtained. Work is proceeding to complete the grid which will be followed by a reacting solution for the entire combustor at the Mach 8 flight condition.

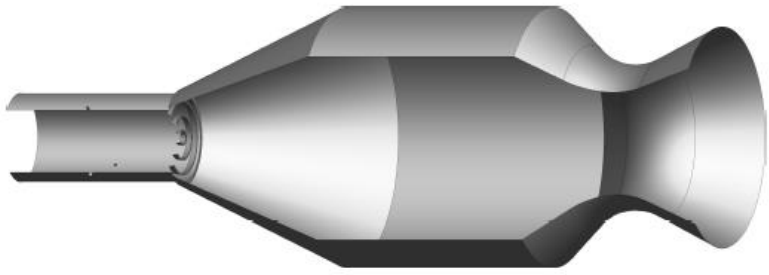

Figure 21. – Three-dimensional geometry used for NCC simulations.

5.0 SUMMARY AND CONCLUSIONS

A new combined-cycle combustor concept employing combustion in a supersonic free-jet was introduced in 2010. A key feature of this combustor is the ability to operate as a traditional ramjet to lower flight Mach numbers than other dual-mode scramjet concepts. The feasibility of supersonic free-jet combustion was shown numerically at flight Mach numbers of 5, 8, and 12 using the GASP code under the assumption of mixing-limited equilibrium combustion. The analysis was subsequently refined using the TAFI code to generate time-accurate solutions with a pre-mixed fuel-air inflow and finite-rate chemistry.

In every case, the reacting supersonic free-jet traversed the combustion chamber and re-joined the nozzle flow surface at the combustor exit. In all cases, the recirculation zone surrounding the jet equilibrated to a pressure higher than that at the inflow. This, combined with the superimposed heat release due to combustion resulted in a periodic wave structure in the jet. In the finite-rate TAFI calculations, the combustion process was enhanced by shock waves in the free-jet, resulting in heat release distributions that were less gradual than those of the mixing-limited GASP results. Uniform and non-uniform fuel inflow profiles were used in the TAFI analysis. The uniform and least non-uniform profile cases converged to time-periodic solutions due to interactions between the free-jet fluid dynamics, combustion chamber pressure, and ignition kinetics. The effect of reducing the nozzle throat area was to increase the combustion chamber pressure, and reduce the period of the wave structure in the free-jet. This was apparent in both sets of calculations.

Temperatures in the recirculation zone surrounding the jet, which determine the fuel heat load were found to depend on the fuel-air ratio in proximity to the shear layer. This was varied by the placement of fuel injectors in the mixing-limited GASP calculations, and by the degree of fuel-air ratio non-uniformity in the TAFI calculations. For a wall temperature of 3000^0R, fuel heat load is well within the capability of hydrocarbon fuels. Wall temperature can be reduced to 2000^0R with endothermic hydrocarbon fuel.

Additional TAFI calculations were done to explore various aspects of the free-jet combustor concept. Results with a single flameholder showed little difference in performance, leading to the conclusion that flameholder drag is not a significant contributor to momentum deficit. Results with a reduced combustion chamber diameter also showed little difference in performance, but lowered heat load in proportion to wetted area. Finally, the Mach 8 geometry was subjected to inflow conditions representative of Mach 10 flight conditions, showing that a fixed-geometry system could operate over a range of flight Mach numbers. Net thrust based on the TAFI results was generally lower than that based on the GASP results. This is attributed to higher momentum loss in the shock-induced combustion process. TAFI-based thrust levels were 17-23% below ideal values at the same combustion pressure ratio.

REFERENCES

[1] WEBER, R.J. AND MACKAY, J.S., "An Analysis of Ramjet Engines Using Supersonic Combustion," NACA Technical Note 4386, August 20, 1958.

[2] FERRI, A., "Possible Directions of Future Research in Air-Breathing Engines," *Combustion and Propulsion*, Fourth AGARD Colloquium, High Mach Number Air-Breathing Engines, Milan, April 4-8, 1960; Editors A.L. Jaumotte, A.H. Lefebre, A.M. Rothrock, Pergamon Press, pp. 3-15, 1961.

[3] DUGGER, G.L., "Comparison of Hypersonic Ramjet Engines with Subsonic and Supersonic Combustion," *Combustion and Propulsion*, Fourth AGARD Colloquium, High Mach Number Air-Breathing Engines, Milan, April 4-8, 1960 Editors A.L. Jaumotte, A.H. Lefebre, A.M. Rothrock, Pergamon Press, pp. 84-119, 1961.

[4] CURRAN, E.T. AND STULL, F.D, U.S. Patent 3,667,233, "Dual Mode Supersonic Combustion Ramjet Engine," June 6, 1972.

[5] TREFNY, C.J. AND DIPPOLD, V.F. III, "Supersonic Free-Jet Combustion in a Ramjet Burner," *46th AIAA/ASME/SAE/ASEE Joint Propulsion Conference & Exhibit*, 25-28 July, 2010, Nashville, TN, AIAA 2010-6643.

[6] TREFNY, C.J. AND YUNGSTER, S., "Free-Jet Combustor Simulation at Mach 8 Flight Condition," *Proceedings of the 35th JANNAF Airbreathing Propulsion Subcommittee Mtg.*, 16-19 May, 2016, Newport News, VA, Paper No. 4494.

[7] PANDOLFINI, PETER P. AND FRIEDMAN, MURRAY A., "Instructions for Using Ramjet Performance Analysis (RJPA)," IBM-PC Version 1.24, The Johns Hopkins University Applied Physics Laboratory, JHU/APL AL-92-P175, 1992.

[8] GASP Version 5 Technical Reference, Aerosoft, Inc., http://www.aerosoftinc.com

[9] YUNGSTER, S. AND RADHAKRISHNAN, K., "A Fully Implicit Time Accurate Method for Hypersonic Combustion: Application to Shock-Induced Combustion Instability," *Shock Waves*, vol. 5, 293-303, 1996.

[10] YUNGSTER, S. AND RADHAKRISHNAN, K., "Pulsating one-dimensional detonations in hydrogen-air mixtures," *Combustion Theory and Modeling*, vol. 8, 745-770, 2004.

[11] SINGH, D.J. AND JACHIMOWSKI, C.J., "Quasiglobal Reaction Model for Ethylene Combustion," *AIAA Journal*, vol. 32, no. 1, pp 213-216, 1994.

[12] LANDER, H. AND NIXON, A.C., "Endothermic Fuels for Hypersonic Vehicles," *Journal of Aircraft*, vol. 8, no. 4, pp. 200-207, 1971.

[13] STUBBS, R.M. AND LIU, N.-S., "Preview of the National Combustion Code," *33rd AIAA/ASME/SAE/ASEE Joint Propulsion Conference & Exhibit*, July 6-9, 1997, Seattle, WA, AIAA 97-3114.

[14] IANNETTI, A., TACINA, R., JENG, S.-M., AND CAI, J., "Towards Accurate Prediction of Turbulent, Three-Dimensional, Recirculating Flows with the NCC," *39th AIAA Aerospace Sciences Meeting & Exhibit*, 8-11 January, 2001, Reno, NV, NASA TM-2001-210761, AIAA–2001–0809.

[15] POVINELLI, F. P., AND POVINELLI, L. A., "Correlation of Secondary and Supersonic Gaseous Jet Penetration into Supersonic Crossflows," NASA TN D-6370, 1971.